

Restoration of Brick and Stone Relief from Single Rubbing Images

Zhuwen Li, Song Wang, Jinhui Yu, and Kwan-Liu Ma, *Senior Member, IEEE*

Abstract—We present a two-level approach for height map estimation from single images, aiming at restoring brick and stone relief (BSR) from their rubbing images in a visually plausible manner. In our approach, the base relief of the low frequency component is estimated automatically with a partial differential equation (PDE)-based mesh deformation scheme. A few vertices near the central area of the object region are selected and assigned with heights estimated by an erosion-based contour map. These vertices together with object boundary vertices, boundary normals as well as the partial differential properties of the mesh are taken as constraints to deform the mesh by minimizing a least-squares error functional. The high frequency detail is estimated directly from rubbing images automatically or optionally with minimal interactive processing. The final height map for a restored BSR is obtained by blending height maps of the base relief and high frequency detail. We demonstrate that our method can not only successfully restore several BSR maps from their rubbing images, but also restore some relief-like surfaces from photographic images.

Index Terms—3D modeling, geometric constraints, restoration, relief, rubbing images, cultural heritage.

1 INTRODUCTION

BRICK and stone relief (BSR) is a form of sculpting where pictures are chiseled into the surface of brick or stone to create something that resembles a combination of both painting and relief. This particular art form was used in ancestral halls and tombs as architectural decorations in the ancient time of China. It emerged in the Warring States period (475-221BCE) and became very popular in the Han Dynasty (206BCE-220AD). BSR provides historical information unavailable elsewhere, paying tribute to local personages by setting down their careers and deeds, or recording local events, military campaigns and victories, charitable subscriptions to religious institutions, etc. A photograph of BSR representing an acrobatic show is given in Fig. 1a.

By the beginning of the seventh century, the Chinese had found a method of making multiple copies of old inscribed records, using handmade rice paper and ink. To make a rubbing of a BSR, a sheet of moistened paper is laid on the inscribed surface of BSR and tamped into every depression with a rabbit's-hair brush. When the paper is almost dry, its surface is tapped with an inked pad, black marks are left on the paper to form rubbing images. Fig. 1b shows a rubbing image of the acrobatic show.

Our goal is to plausibly restore the relief surface of BSR from their rubbings (Fig. 1c). This study is an important endeavor in promoting not only fragmented, stolen, or lost BSR but also existing BSR, as it allows viewers to appreciate the 3D appearance of ancient BSR by changing views and lighting conditions, in a manner better than looking at 2D

rubbings and photographs. From the application perspective, our work can be applied in a wide range of areas ranging from digital libraries, digital museums, milling, embossment, sculpting to packaging.

We propose a method in this paper to restore the BSR surface by a height map estimation scheme which consists of two levels: the *base relief* (BaseRLF), referring to the low frequency component of BSR surface, and the *high frequency detail* (HFDetail), referring to small local features and randomness of BSR surface. The overall architecture of our system is presented in Fig. 2. A detailed description of the workflow is given in the figure caption.

2 RELATED WORK

Our work falls broadly into the area of 3D reconstruction from a single image. Reconstructing a 3D object from a single 2D image is an ill-posed problem. A monocular image alone does not contain sufficient information to uniquely retrieve 3D information; however, the third dimension can be recovered from monocular images in conjunction with certain visual cues (e.g., size, shade, distortion, and vanishing points) or prior knowledge of certain geometric properties of the object. Based on those cues, many algorithms have been proposed for the 3D reconstruction from single images in very specific settings.

Methods such as shape from shading [1], [2], [3] are based on the theory that the intensity of a pixel is determined in part by the angle between the surface normal and the illumination direction. Interactive methods [4], [5], [6] recover surface normals by having the user specify absolute surface positions or absolute surface normals as constraints. A shading-based surface editing approach was proposed in [7]. Karpenko and Hughes [8] introduced a system for estimating 3D smooth surfaces from visible counter surfaces. Wu et al. [9] introduced an interactive approach to recover the overall global structure-based normal reconstruction for local image region.

The shape from texture techniques [10], [11], [12], [13] uses cues from the image plane variations in the texture

- Z. Li, S. Wang, and J. Yu are with the State Key Lab of CAD&CG, Zhejiang University, Hangzhou 310027, China. E-mail: {lizhuwen, wangsong, jhyu}@cad.zju.edu.cn.
- K.-L. Ma is with the Department of Computer Science, University of California-Davis, 2063 Kemper Hall, One Shields Avenue, Davis, CA 95616-8562. E-mail: ma@cs.ucdavis.edu.

Manuscript received 6 Sept. 2010; revised 1 Dec. 2010; accepted 5 Jan. 2011; published online 26 Jan. 2011.

Recommended for acceptance by J. Stam.

For information on obtaining reprints of this article, please send e-mail to: tcvg@computer.org, and reference IEEECS Log Number TVCG-2010-09-0220. Digital Object Identifier no. 10.1109/TVCG.2011.26.

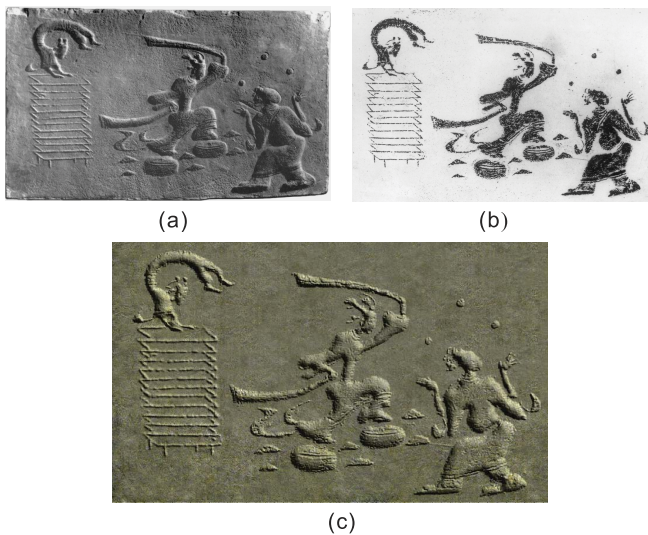


Fig. 1. Acrobatic show. (a) Photograph of BSR. (b) Rubbing image. (c) Restored BSR surface.

properties such as density, size, and orientation. The orientation of the surface is measured by the maximum change in the primitive size of the known texture elements. Other methods [14], [15], [16], [17], [18], [19] reconstruct a 3D geometric entity from a single image in conjunction with geometric constraints on the 3D geometric entity.

Nayar and Nakagawa [20] recovered depth information by estimating the amount of blur in the image. Single view metrology [21] assumes that vanishing lines and points are known in a scene, and calculates angles between parallel lines to infer 3D structure from Manhattan images. A supervised learning approach to 3D depth estimation from a single image is presented in [22] and [23].

The traditional emboss algorithm computes gradient vectors for each pixel in the input image. The resultant image is embossed with a very *shallow* depth because the gradient computation in essence performs a high pass filtering (see Fig. 6b). Miller [24] proposed an idea of surface accessibility which measures the ability of a spherical probe to enter a structure from outside as well as to fit locally on the surface.

As for bas-relief generation, an older paper [25] gives a basic approach that treats bas-relief generation as a problem of embossing on the view plane. Most recently, some researchers [26], [27], [28] noted a similarity between bas-relief generation and high dynamic range (HDR) imaging, and compressed range of intensities in such a way to retain detail in both shadows and highlights. In relief processing, depth replaces the intensities in HDR. The feature sensitive approach [29] operates in the gradient domain and makes use of different binary masks in order to identify pixels which belong to sensitive parts of the height field. Sun et al. [30] proposed a method to automatically generate bas-relief based on adaptive histogram equalization, starting from an input height field.

Most of existing 3D reconstruction methods and bas-relief generation techniques are not suited for BSR restoration because:

1. There is no lighting/continuous shading, focus, and perspective information available on rubbings.
2. Textures depicting raised objects on rubbings are not regular as required in shape from texture techniques but random.
3. Aforementioned bas-relief generation methods take 3D models as input, while our restoration starts from 2D rubbing images.
4. The original BSR objects have been lost or stolen, or have been fragmented and reside in various repositories and institutions around the world. Numerous objects are in private collections and are not open to public view. Relying on 3D scanning to get BSR surface is impractical.

Our BSR surface restoration scheme is partially inspired by the idea of separating low and high frequency components in the interactive normal reconstruction [9], in which the high frequency component is estimated by a shape from shading algorithm, and the low frequency component is recovered *manually*. In our approach, however, the low frequency component is estimated *automatically* and the high frequency component is recovered either automatically or optionally with minimal user interventions.

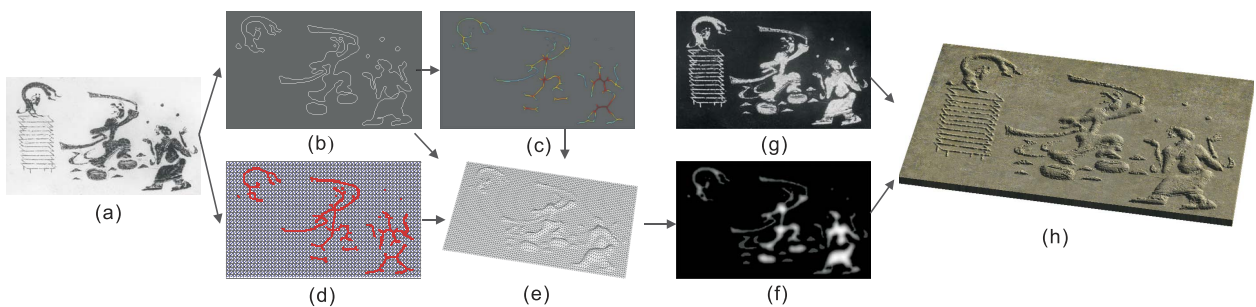


Fig. 2. System workflow overview. In the base relief height map estimation, we first input a rubbing image (a) and detect object regions on rubbing images (b), skeletons inside the object regions are abstracted and assigned with heights estimated by an erosion-based contour map (c). Next, we construct a triangulation mesh over the rubbing image and select vertices on the mesh that are close to the skeleton abstracted (d), the heights on the skeleton are transferred onto selected vertices to form height constraints. These height constraints, together with positions, normals of vertices near the object boundary on the mesh are taken as boundary conditions to deform the mesh by a partial differential equation (PDE)-based approach (e). The deformed mesh is converted into a height map for the base relief (f). In the high frequency height map estimation, we invert rubbing image pixel values as the height map of high frequency detail (g). The final height map of restored BSR is obtained by summing up two estimated height maps with a simple formula. The system output is the restored relief surface rendered with BSR textures (h).

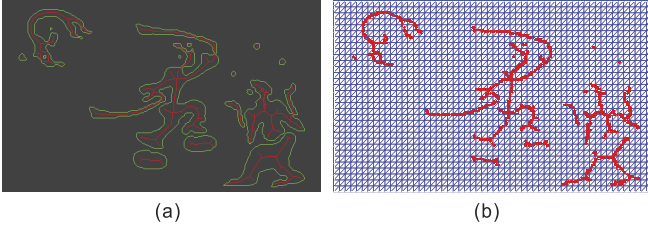


Fig. 3. (a) Object region contour and skeleton. (b) Selected constraint vertices.

3 HEIGHT MAP ESTIMATION OF THE BASE RELIEF

Our height map estimation for the base relief involves detection of object regions on rubbing images, determination of height constraints, PDE-based mesh deformation, and conversion from 3D mesh to height map.

3.1 Detection of Object Regions on Rubbing Images

Object images on rubbings are depicted by denser random marks, so applying a boundary detection (BdD) algorithm straightforwardly to the rubbing image may pick up some marks inside object regions. In order to get the whole object boundary rather than the individual mark boundary inside object regions, we resize the rubbing picture into a smaller percentage of its original size so that denser marks form almost continuous dark regions resembling original object images on rubbings. Let I be an input rubbing image of its original size and I' its small version, we apply the snake algorithm [31] to segment I' into K disjoint regions which can be further divided into $K - 1$ object regions OBR'_i and the background region BKR' by identifying the color inside them.

$$I' = \cup_{k=1}^{K-1} OBR'_k + BKR'. \quad (1)$$

For some rubbings, after the snake algorithm is applied, a few holes may appear inside OBR'_k due to noises of random marks on rubbing images (as shown in the accompanying video, which can be found on the Computer Society Digital Library at <http://doi.ieeecomputersociety.org/10.1109/TVCG.2011.26>). Those holes are not desirable for our restoration task because our system will take them as object boundaries. We therefore require users to remove them via an interactive interface. (More details about the interactive tools provided by our system are given in Section 4.)

The boundary points associated with OBR'_k in I' are then mapped onto I . We interpolate those boundary points with a cubic spline to get a curve that draws corresponding object region OBR_k on I , as shown by green curves in Fig. 3a.

After object regions are obtained, we lay a floating-point grid over the rubbing image. The grid cell size is 1 pixel wide so that a one-to-one correspondence between the grid vertices and the pixels of the rubbing image can be established. On each grid cell, a diagonal line is added so that we can get a triangulation mesh $M(P, E)$ for the base relief surface to be estimated, where P is a set of N vertex positions, $P = \{\mathbf{p}_i \in R^3 \mid 1 \leq i \leq N\}$, and $E = \{(i, j) \mid \mathbf{p}_i \text{ is connected to } \mathbf{p}_j\}$ is the set of edges. Note that the height value (z -coordinate) of each vertex on the triangulation mesh is initially assigned with 0.0. Since the background of BSR is flat, only the mesh inside OBR_k needs to be deformed. We consequently calculate the intersection between vertices on $M(P, E)$ and pixels inside OBR_k to

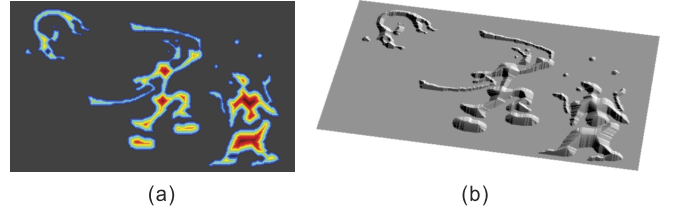


Fig. 4. (a) Contour map. (b) Height surface with shading.

obtain submeshes $M_k(P, E)$ which are then deformed with the method described next.

3.2 Automatic Determination of Height Constraints

In the PDE-based mesh deformation approach, the mesh is divided into three parts: a *handle region*, an *interpolation region*, and a *fixed region*. Positions of the handle and fixed vertices and the differential properties of the surface are treated as boundary conditions to deform the mesh.

Height constraints in our case refer to those vertices in the handle region, which define the target features of the surface to be deformed. In most mesh editing systems, handle vertices are specified by the user *manually* for editing purposes, while in our system, the height constraints are determined *automatically*. This involves an automatic selection of some vertices inside OBR_k and automatic determination of their heights.

In shape analysis, the skeleton of a shape is its thin version that is equidistant to its boundary. The skeleton emphasizes the geometrical and topological properties of the shape and thus is a good candidate for guiding the selection of handle vertices. We adopt the traditional skeleton algorithm on OBR_k to obtain their skeletons. Usually, the skeleton abstracted has subbranches that touch the OBR_k boundary. Such touch may lead to small but visible ridges on the deformed mesh near the OBR_k boundary. We store the pixels on the skeleton in a tree data structure and delete a few pixels on the skeleton that are near the OBR_k boundary. From our experiments, we found that for images with size ranging from 400 to 800 pixels, deleting 4 pixels is adequate for eliminating visible ridges on deformed surface. Remaining pixels on the skeleton are indicated with red color in Fig. 3a. Next, we use a 3×3 window to trace remaining pixels on the skeleton. Vertices on $M_k(P, E)$ falling into the window are selected as candidates of constraint vertices (red dots in Fig. 3b). Since all vertices on the mesh $M_k(P, E)$ are initially assigned with 0.0 height in the triangulation process, we need to raise heights of selected constraint vertices to the expected positions for mesh deformation.

Determination of heights for vertices in the handle region is not an easy task because the boundary of OBR_k is irregular in shape and it is hard to find a suitable reference axis to define heights for vertices in the handle region. Our solution to this problem is to construct a reference height map inside OBR_k by applying the traditional erosion algorithm over OBR_k . Since the erosion algorithm erodes away the boundary of the region, we take eroded boundary as an isohypse and assign a color to the isohypse to indicate its height. We continue such operations over the eroded region until the region shrinks to zero. In the end, a contour map is obtained as shown in Fig. 4a. Corresponding height surface with shading is given in Fig. 4b.

Since heights corresponding to central positions of OBR_k on the reference height map are proportional to the times of

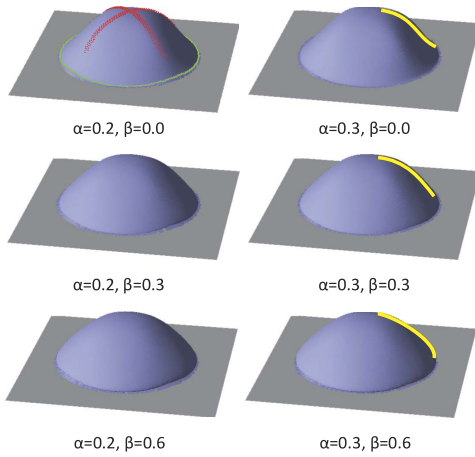


Fig. 5. Results of deformed mesh in a circular region under varying weights.

erosion applied to OBR_k , heights on narrow parts of OBR_k appear reasonably lower than those on wider parts. Such height variations on central parts of OBR_k look plausibly consistent with most of BSR, as demonstrated by Fig. 4 as well as some other examples given in Section 6.

Drawbacks of the reference height map are: 1) the slope of raised parts inside OBR_k is almost linear, while the raised slope of BSR should be curved, and 2) some arrises appear on the height surface. Because erosion is performed pixel by pixel on the boundary of OBR_k , the sawtooth effect on each isohypse results in arrises on raised height surface.

To overcome these two drawbacks associated with the reference height map, we calculate the union of the skeleton and the reference height map to get a skeleton with height information encoded by colors (Fig. 2c), and then transfer the height information onto vertices close to the skeleton in the handle region on $M_k(P, E)$ to get height constraints. We impose height constraints, boundary position, and normal constraints into the PDE-based mesh deformation system, described in the next section, to obtain a mesh with more natural look on raised parts inside OBR_k .

3.3 PDE-Based Mesh Deformation

Existing PDE-based approaches are categorized as nonlinear and linear methods. Nonlinear methods solve Laplacian or Poisson equations using nonlinear iterative solvers [32], [33], [34], [35], [36]. These methods produce fair surfaces, but they are time consuming. Linear PDE-based approaches encode Laplacians and positional constraints in a linear system and obtain the deformed shapes by solving the linear system [37], [38]. Since our application involves no large rotation on the deformed region, we adopt the fast linear PDE-based approach. A discrete Laplacian δ_i on mesh $M_k(P, E)$ is defined at each point by the weighted sum of difference vectors between the point and its adjacent neighbors:

$$\delta_i = \mathbf{p}_i - \sum_{j \in N(i)} w_{ij} \mathbf{p}_j, \quad (2)$$

where $N(i) = \{j \mid \{i, j\} \in E\}$ are the edge neighbors, w_{ij} is the weight for point \mathbf{p}_j . The weights w_{ij} are assigned as cotangent weight given [33]. We can write (2) in a matrix form:

$$\delta = LP, \quad (3)$$

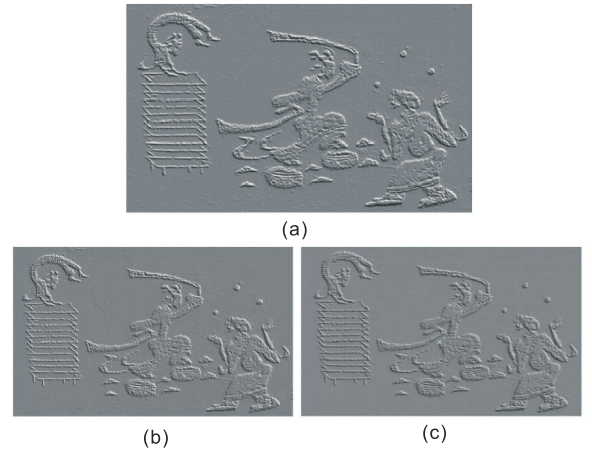


Fig. 6. High frequency detail estimated by (a) our method, (b) traditional emboss algorithm, and (c) shape from shading technique.

where δ is composed of δ_i and P is composed of p_i . The matrix L is commonly considered as the Laplacian operator of the mesh and L has rank $N_k - 1$ (N_k is the number of vertices in $M_k(P, E)$), which means P can be recovered from δ by fixing one vertex and solving a linear system.

The approach to performing deformations using Laplacian coordinates δ_i is to fix the absolute position of several vertices (see [39]), i.e.,

$$\mathbf{p}'_i = \mathbf{q}_i, i \in \{m, \dots, N_k\}, m < N_k, \quad (4)$$

and solve for the remaining vertices $\{\mathbf{p}'_i, i \in \{1, \dots, m-1\}\}$ by fitting the Laplacian coordinates of geometry P' to the given Laplacians δ_i . It has been observed that the solution behaves better if the constraints \mathbf{q}_i are satisfied in a least-squares sense rather than exactly [40], [41]. This results in the following error functional:

$$E(P') = \sum_{i=1}^{N_k} \|L(\mathbf{p}'_i) - \delta_i\|^2 + \alpha \sum_{i \in H+F} \|\mathbf{p}'_i - \mathbf{q}_i\|^2, \quad (5)$$

where H and F are the handle and fixed sets, respectively. Equation 5 has to be minimized to find a suitable set of coordinates P' . The first term is supposed to preserve local details on the mesh surface. The second term enforces positions of handle and fixed vertices. α is a weight with which users can tune the deformed surface.

Although (5) is adequate for most of mesh editing applications, the resultant surfaces are not satisfactory for our BSR restoration, as illustrated by deformed surfaces in a circular region on the top row of Fig. 5, where red dots indicate height constraints derived from the skeleton abstracted from the circle, and green dots indicate fixed boundary vertices of the circular region.

First, the deformed surface has a concave up slope (as indicated by the yellow curve on top row in Fig. 5) near the object boundary, while the slope of raised parts on BSR should be concave down. Second, the deformed surface appears higher near the handle region and lower far from the handle region. It is expected in BSR restoration that the lower parts far from the handle should be raised equally as those parts near the handle region. In order to get better approximation of the base relief surface, we add an additional term in the energy function in (5) to enforce the normal of fixed vertices on the object boundary:

$$E(P') = \sum_{i=1}^{N_k} \|L(\mathbf{p}'_i) - \delta_i\|^2 + \alpha \sum_{i \in H+F} \|\mathbf{p}'_i - \mathbf{q}_i\|^2 + \beta \sum_{i \in F} \|\mathbf{n}'_i - \mathbf{n}_i\|^2. \quad (6)$$

In our implementation, we let the normal along the boundary of OBR_k lay on the background plane, pointing outward. The weight β is used to balance users objectives. Next, we examine the influences of varying weights.

Fig. 5 shows results with α increasing from left to right column, and β increasing from top to bottom row. It can be seen that $\alpha = 0.2$ may lead to the deformed mesh exceeding a little bit the original boundary. Such exceeding phenomena become weak when constraints on the set H and F are further enforced with $\alpha = 0.3$, while over weight on α may lead to ineffectiveness of normal constraints in (6).

The addition of normal constraints on the fixed set improves deformation results in two aspects as we expected. First, the slope of raised surface becomes concave down after normal constraints are added. Second, the lower parts far from the handle are raised further with β increases. But overweight on β may cause the slope of raised parts curving inward near the OBR_k boundary and the deformed surface succeeding the object boundary (third row in Fig. 5). A moderate deformed surface can be obtained by balancing two weights with $\alpha = 0.3$ and $\beta = 0.3$, as shown by second row on the right column in Fig. 5 as well as other examples shown in Section 6.

3.4 Conversion from 3D Mesh to Height Map

Since our high frequency detail is easy to be estimated with a height map (described in next section), we need to convert the 3D mesh for the base relief to a height map so that the final height map can be obtained by summing the height map of both base relief and high frequency detail.

To do this, we first check which triangle a height map pixel falls, and then apply bilinear interpolation inside the triangle on the mesh. Once all heights corresponding to height map points are interpolated, a complete height map for the base relief is obtained, as shown in Fig. 2f. Note that the ladder under the left person is removed from the base relief height map, because the ladder is taken as part of high frequency detail, which is processed with the method described in the next section.

4 ESTIMATION OF HIGH FREQUENCY DETAIL

Black marks on rubbings record the boundary of object figures, small local features, and random appearance of BSR surface. White areas on rubbings correspond to small gaps among black marks and the background of BSR. Pixel values on rubbing images themselves in some degree thus reflect height variations of high frequency component of BSR. Consequently, we take the rubbing image directly as an estimation of the height map for high frequency detail by simply inverting pixel values on the rubbing image, as shown by Fig. 2g and a shaded version in Fig. 6a.

For comparison, we include results of applying the traditional emboss algorithm and shape from shading technique to the rubbing image, as shown in Figs. 6b and 6c. Visually, three images look similar because they all show the emboss effect with very shallow depth, which is unable to represent the low frequency components of the base relief

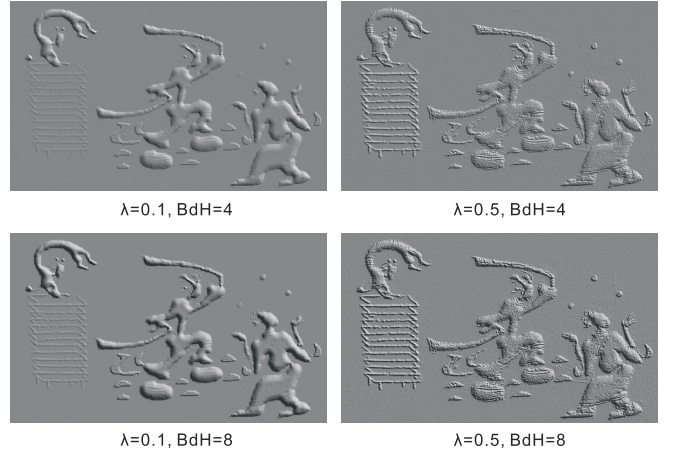


Fig. 7. Results of restored BSR with varying settings on λ and BdH .

evident in Fig. 7 and can only be used to estimate high frequency detail.

Our experiments show that for some rubbing images, the high frequency detail estimated automatically is adequate for the restoration task, such as the examples given in Figs. 10, 11, and 13 in Section 6. While for some other rubbing images, a little interactive processing is needed to get better estimation for high frequency detail. Take the acrobatic show as an example, some small spots on human body appear a little bit deeper and the ladder appears thinner than expected. In the system, we provide a few tools which allow users to modify the rubbing image for their objectives.

The first one is the polygon drawing tool with which users may select some area of interest on rubbing images. The area surrounded by the polygon can be taken as a mask that either allows further processing on pixels inside the area or prevents pixels inside the area from being processed. Some conventional processing such as dilation, erosion, deletion, etc., can be applied to the pixels inside the selected region. As for small gaps among black marks inside OBR_i , we detect them by comparing their areas with an adjustable threshold and modify values of pixels falling into those gaps by multiplying them with a constant $k_1 < 1$. Users may tune the k_1 value until the height in detected gaps looks fine in the estimated high frequency detail.

5 SUMMATION OF TWO HEIGHT MAPS

We denote the two height maps obtained previously with M_b for the base relief and M_h for high frequency detail. The final height map M_f for restored BSR is obtained by blending two height maps with normalized gray-scale values with the following formula:

$$M_f = (1 - \lambda)M_b + \lambda M_h, \quad (7)$$

where λ is a blending factor. We sample M_f at pixel resolution and create a 3D mesh consisting of connected triangles to obtain the restored BSR surface $M_n(P, E)$ with normalized height. The final restored BSR surface $M_f(P, E)$ with absolute height can be obtained by multiplying z -coordinate values of vertices on $M_n(P, E)$ with a factor BdH for the relief bounding height.

Fig. 7 shows results of restored acrobatic show with λ increasing from left to right column, and BdH increasing

TABLE 1
Summary of Processing Time

	Image size	BdD (sec)	BaseRLF (sec)	HFDdetail (sec)	Int (min)
Acrobatic show	700 × 420	5.2	58.1	.12	~2
Camel	630 × 534	5.8	78.7	.1	~3
Dragon	800 × 386	5.6	46.7	.18	~2
Tiger	800 × 402	4.7	46.2	.16	0
Egyptian relief	426 × 545	6.1	73.3	.12	0
Ballet dancer	434 × 600	2.8	67.6	.05	~3
Crane	697 × 653	5.2	88.2	.06	0

from top to bottom row. We can see that a smaller λ leads to attenuation of fine details and increasing the base relief, while a bigger λ leads to amplification of high frequencies and reduction of the coarse shape variations. The influence

of varying BdH on the absolute height of $M_f(P, E)$ is obvious. In our system, the default value of λ is set to 0.3, which would produce satisfactory results for most of our restoration tasks. In addition to BSR restoration, users may further edit the relief surface by altering λ and BdH to meet their artistic demands.

6 RESULTS

In this section, we present some results of restoring BSR from their rubbings. Our system is implemented with Matlab 7.5 and run on a PC with Pentium 2.8 GHz CPU and 4 GB memory. Table 1 tabulates the processing time involved in boundary detection, height map estimation for the base relief and high frequency detail, and interaction (Int).

Acrobatic show. Fig. 1c shows the result of restored acrobatic show BSR. In this example, we detect small gaps

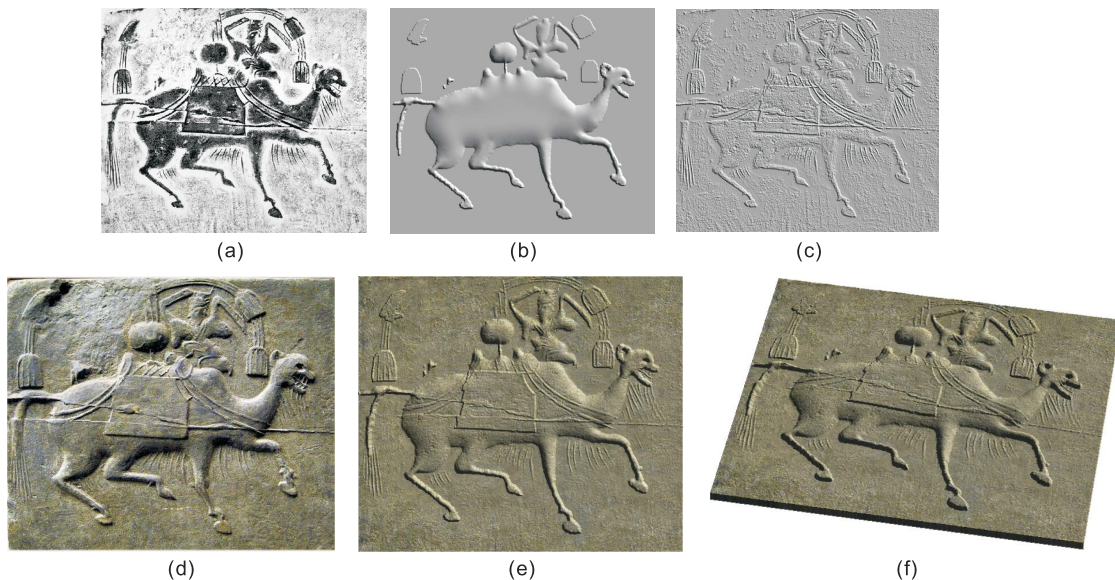


Fig. 8. Drumming on a camel: (a) Rubbing image. (b) Base relief. (c) High frequency detail. (d) Photograph. (e) and (f) Two views of restored relief.

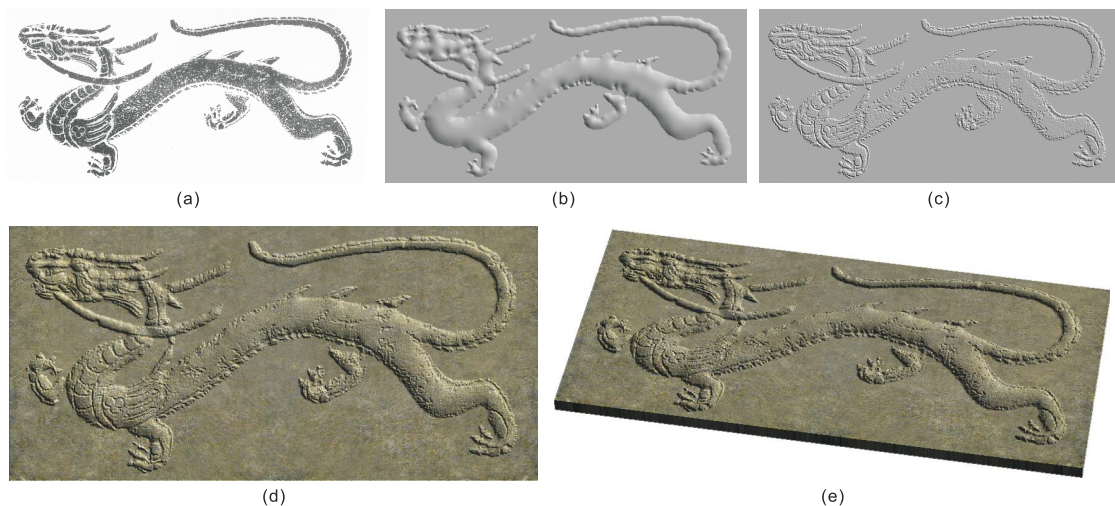


Fig. 9. Dragon: (a) Rubbing image. (b) Base relief. (c) High frequency detail. (d) and (e) Two views of restored dragon.

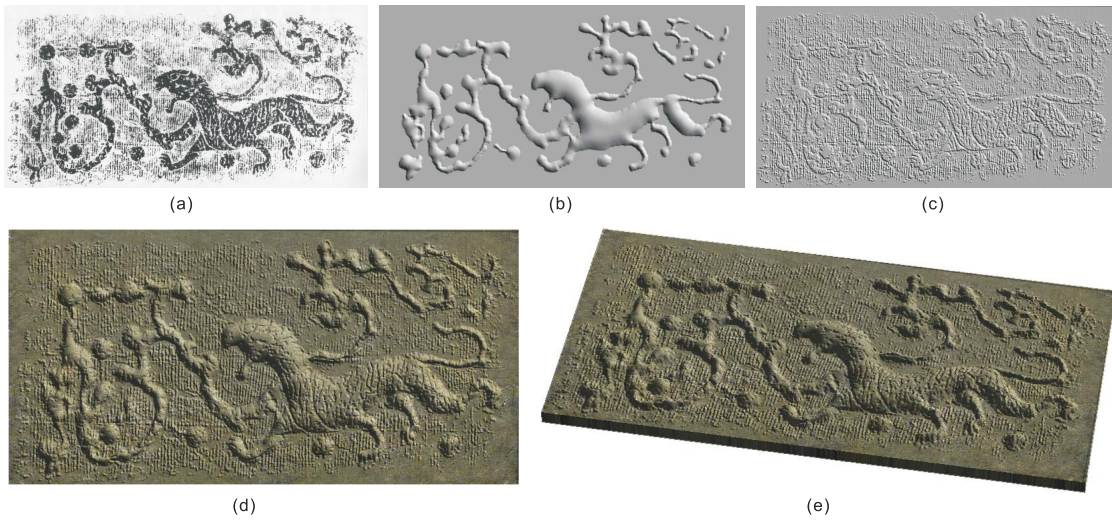


Fig. 10. Tiger: (a) Rubbing image. (b) Base relief. (c) High frequency detail. (d) and (e) Two views of restored tiger.

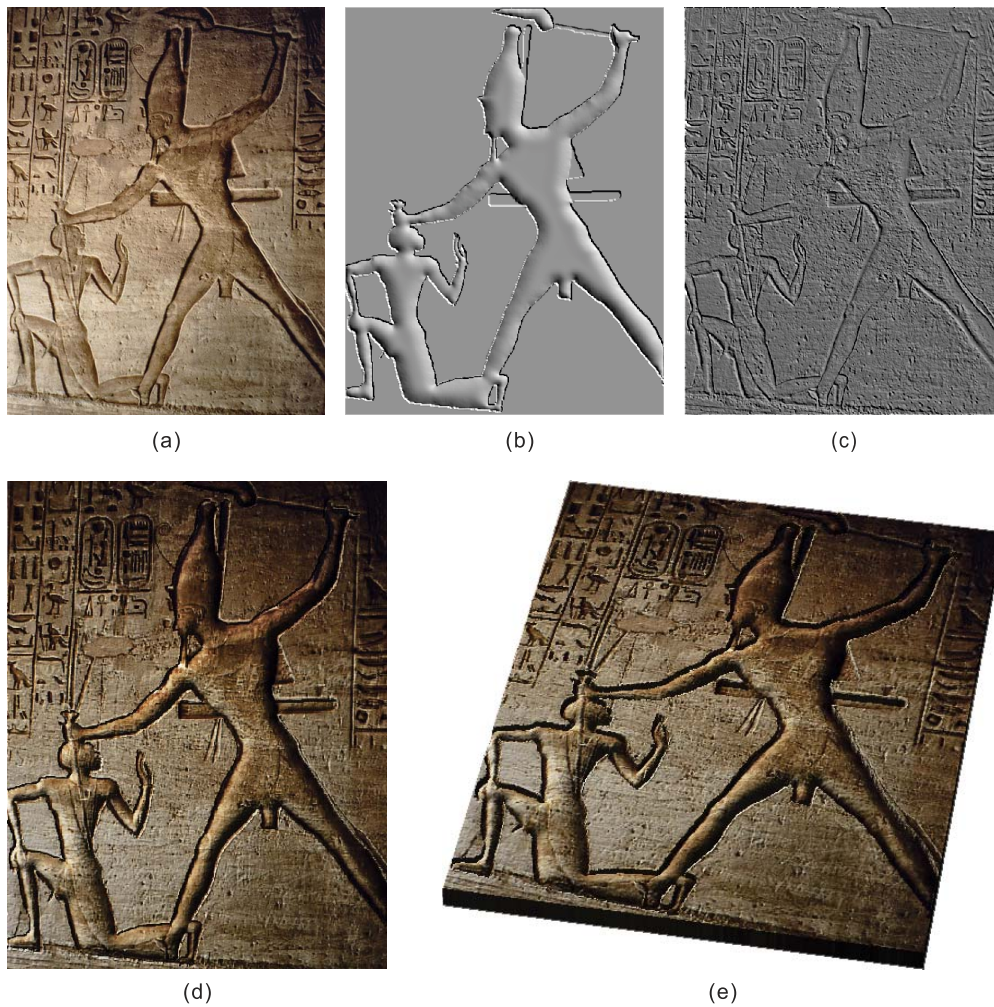


Fig. 11. Egyptian relief. (a) Photograph. (b) Base relief. (c) High frequency detail. (d) and (e) Two views of restored Egyptian relief.

among black marks with proper threshold so that only values of pixels falling in spotty gaps are modified, and pixels falling in stripy gaps on drum-like objects beneath

the foot of the middle person remain unchanged. As a result, stripy gaps as decorative patterns are reasonably deeper than spotty gaps in the restored surface. In order to

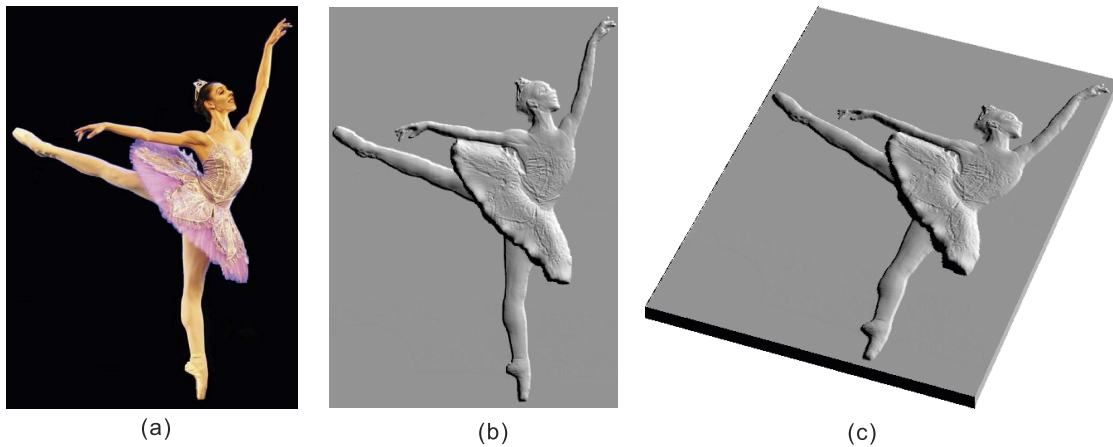


Fig. 12. Ballet dancer. (a) Photograph. (b) and (c) Two views of ballet dancer relief.

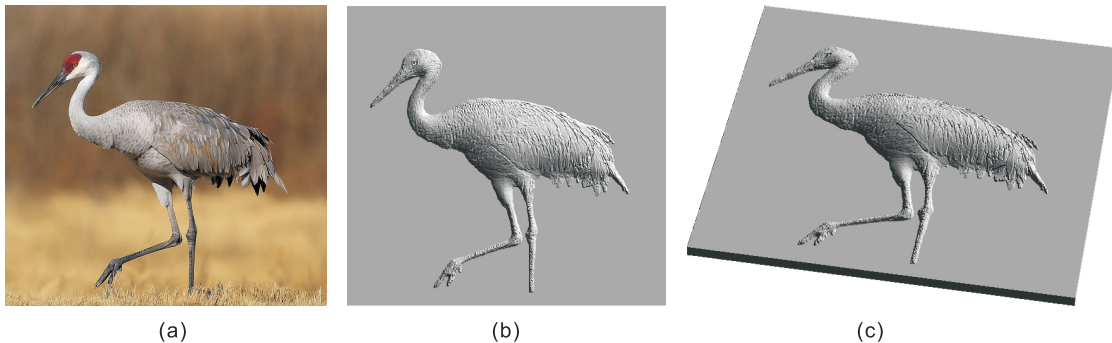


Fig. 13. Crane. (a) Photograph. (b) and (c) Two views of crane relief.

enhance the visual quality, we map the textures synthesized manually from BSR relief photographs onto the restored surface (the same textures are also used in the next three examples). Compared with the photograph (Fig. 1a), the restored acrobatic show looks satisfactory.

Drumming on the camel. In Fig. 8d, we show a stone relief photograph drumming on the camel. This stone relief was damaged so that some objects on the upper left were missing. It appears that the drumming person is lower than the camel. With our current base relief restoration scheme, the maximum heights of restored drumming person are the same as camel's, which is not desirable compared with the photograph in Fig. 8d. Fortunately, the additive nature of our height map estimation scheme offers support to additional layers for improving the estimation of the base relief of different objects on BSR. Take the drumming person for instance, we can use a separate layer to estimate its heights, and add it with a lower weight to the base relief of other objects obtained with the former estimation scheme.

Note that the surface of the damaged portion looks irregular on the photograph. Such irregular surfaces cannot be restored with our system because no distinct edge can be found for the damaged area on the rubbing image and no prior knowledge is available for the irregular surface. We treat the damaged portion as the background instead.

Dragon and tiger. Next, we show results of restored dragon and tiger relief (Figs. 9 and 10). Unfortunately, there are no photographs available for these two examples. On the restored dragon surface, some shallow patterns inscribed lower than the raised BSR surface such as those around the neck of dragon are also well preserved. The heights of spotty gaps around the middle part of the dragon's body are raised interactively close to the surface. In Fig. 10, the original stone relief indicates a group of seven stars in the western sky named as a tiger in ancient China. Thin vertical patterns carved on the background are estimated as part of the high frequency detail.

Although our initial aim is to restore BSR from rubbing images, our system is also able to "restore" the relief effects of object in photographs, *as long as their contours are detectable*. In the case that photographs are used as the input, we convert the color photographs into gray-scale

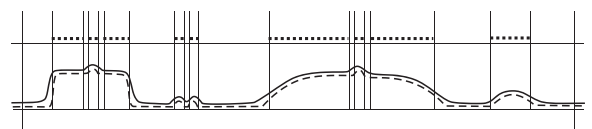


Fig. 14. Illustration of BSR surface, paper surface, and marks on the rubbing paper.

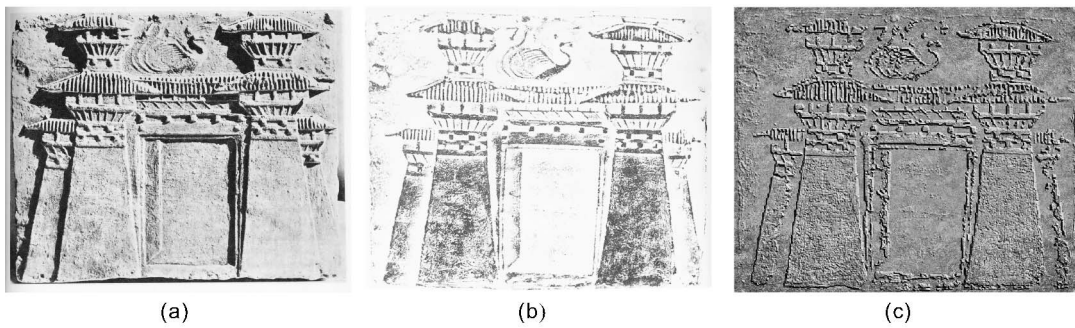


Fig. 15. Lookout building: (a) Photograph. (b) Rubbing image. (c) Restored relief surface.

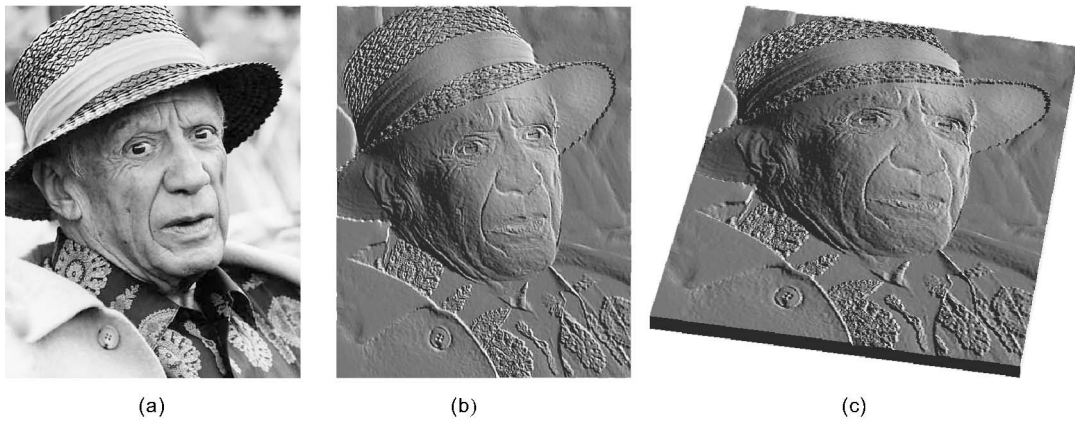


Fig. 16. Picasso: (a) Photograph. (b) and (c) Two views of Picasso's relief.

images which are then used as the estimation of high frequency components, but we do not need to invert pixel values as we would do to rubbing images. Presently, our system is able to restore the relief surfaces from photographic images of objects which are made of homogeneous materials with relatively little texture and albedos. Next, we show three examples of restored relief from photographs.

Egyptian relief. Fig. 11 shows an Egyptian relief. Note that this ancient Egyptian relief used sunken relief in which the design was incised deeper than the background. After object contours are detected, we first restored relief surfaces and then raised the background plane higher. We textured the restored relief with the original photograph and the resultant picture looks quite satisfactory.

Ballet dancer and crane. In Figs. 12 and 13, we show two more examples of restored relief from photographs, a ballet dancer, and a crane. In the example of the ballet dancer, we used a separate layer to treat the tutu by assigning different height constraints on the tutu's boundary so that it appears higher than the body in the restored relief. Note that our system constructs object surfaces with the prior of BSR. The raised surface in Figs. 12 and 13 looks somewhat like a relief rather than the accurate 3D surface of the dancer and crane, so that our system can be used for relief product design by aid of photographic images.

7 LIMITATIONS

It should be pointed out that accurate restoration of BSR from their rubbings is *impossible* because rubbing images are essentially handmade art works. Marks on rubbings are printed under the pressure of the inkpad held by hand.

The resultant rubbing images therefore vary to some degree from artist to artist, and even vary from time to time for an artist who rubs the same BSR. Furthermore, rubbings are a binary transformation of original BSR surface height, as illustrated with a cross section of BSR in Fig. 14, where the dash line, solid curve, and dots indicate the top profile of the cross section, the paper laid on BSR, and marks on rubbings, respectively. Due to the paper tension, it is hard for the rubbing paper to tightly touch corners of raised BSR surface and the background, the object boundary printed on rubbing images is thus slightly apart from the real one on original BSR. Therefore, the restored BSR surfaces with our system are merely plausible approximations of original BSR, as demonstrated by examples in this paper.

Next, we show two unsatisfactory cases of our restoration scheme. The first is a lookout building BSR (Fig. 15a). In the figure, walls on the left and right side are carved with smaller heights compared with those close to the central door, and roofs with vertical patterns are higher than their surrounding parts. Unfortunately, information of such difference in heights on BSR is not available on its rubbing image (Fig. 15b). Our system is thus just able to restore them with the same height. Furthermore, the sharp corners formed by neighboring walls on the lookout building are untouchable during the rubbing process (please refer to Fig. 14) such that our system can only treat them as background (Fig. 15c).

The second is a portrait photograph of Picasso. Our system fails to correctly restore Picasso's face especially on the local concave parts such as eyes and local convex part such as the nose, as shown in Fig. 16. This is because in our

system, we assume that heights of raised surface vary in a way of low-relief BSR.

8 CONCLUSIONS AND FUTURE WORK

Brick stone relief represents a unique form of Chinese art. We present a method for restoring BSR surfaces from single rubbing images. The main contribution of our method is the automatic estimation of height information for each object region with a PDE-based mesh deformation approach. Our method can restore BSR surfaces with a variety of objects ranging from human, animal figures to other decorative patterns of BSR. In addition, our method can also recover relief-like surfaces from photographs. In our future work, we plan to incorporate interactive deformation editing into low frequency surface restoration for obtaining improved results.

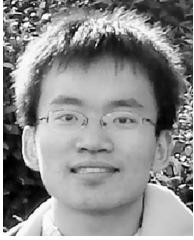
ACKNOWLEDGMENTS

The authors would like to thank the associate editor and all the reviewers for their constructive comments to improve the manuscript. This work is supported by the State Key Program of National Natural Science Foundation of China (No. 60933007), the Key Technologies R&D Program of China (No. 2007BAH11B02), and China Academic Digital Associative Library.

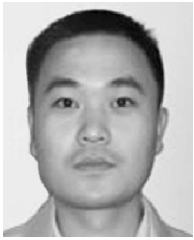
REFERENCES

- [1] R. Zhang, P.-S. Tsai, J.E. Cryer, and M. Shah, "Shape from Shading: A Survey," *IEEE Trans. Pattern Analysis and Machine Intelligence*, vol. 21, no. 8, pp. 690-706, Aug. 1999.
- [2] A. Maki, M. Watanabe, and C. Wiles, "Geotensity: Combining Motion and Lighting for 3D Surface Reconstruction," *Int'l J. Computer Vision*, vol. 48, no. 2, pp. 75-90, 2002.
- [3] M. Glencross, G.J. Ward, C. Jay, J. Liu, F. Melendez, and R. Hubbard, "A Perceptually Validated Model for Surface Depth Hallucination," *ACM Trans. Graphics*, vol. 27, no. 3, pp. 59:1-59:8, Aug. 2008.
- [4] L. Zhang, G. Dugas-Phocion, J. Samson, and S. Seitz, "Single View Modeling of Free-Form Scene," *Proc. IEEE CS Conf. Computer Vision and Pattern Recognition (CVPR '01)*, vol. 1, pp. 990-997, 2001.
- [5] G. Zheng, Y. Matsushita, L. Quan, and H. Shum, "Interactive Shape from Shading," *Proc. IEEE CS Conf. Computer Vision and Pattern Recognition (CVPR '05)*, vol. 1, pp. 343-350, 2005.
- [6] M. Prasad, A. Zisserman, and D.A. Fitzgibbon, "Single View Reconstruction of Curved Surfaces," *Proc. IEEE CS Conf. Computer Vision and Pattern Recognition (CVPR '06)*, vol. 2, pp. 1345-1354, 2006.
- [7] Y. Gingold and D. Zorin, "Shading-Based Surface Editing," *ACM Trans. Graphics*, vol. 27, no. 3, pp. 577-584, 2008.
- [8] O.A. Karpenko and J.F. Hughes, "Smoothsketch: 3D Free-Form Shapes from Complex Sketches," *ACM Trans. Graphics*, vol. 25, no. 3, pp. 577-584, 2006.
- [9] T.-P. Wu, J. Sun, C.-K. Tang, and H.-Y. Shum, "Interactive Normal Reconstruction from a Single Image," *Proc. ACM SIGGRAPH Asia*, vol. 27, no. 5, 2008.
- [10] J. Malik and P. Perona, "Preattentive Texture Discrimination with Early Vision Mechanisms," *J. Optical Soc. of Am.*, vol. 7, no. 5, pp. 923-932, 1990.
- [11] T. Lindeberg and J. Garding, "Shape from Texture from a Multi-Scale Perspective," *Proc. Int'l Conf. Computer Vision (ICCV '93)*, pp. 683-691, 1993.
- [12] J. Malik and R. Rosenholtz, "Computing Local Surface Orientation and Shape from Texture for Curved Surfaces," *Int'l J. Computer Vision*, vol. 23, no. 2, pp. 149-168, 1997.
- [13] B.J. Super and A.C. Bovik, "Shape from Texture Using Local Spectral Moments," *IEEE Trans. Pattern Analysis and Machine Intelligence*, vol. 17, no. 4, pp. 333-343, Apr. 1995.
- [14] R. Jain, R. Kasturi, and B. Schunck, *Machine Vision*. McGraw-Hill, 1995.
- [15] P. Debevec, C. Taylor, and J. Malik, "Facade: Modeling and Rendering Architecture from Photographs," *Proc. ACM SIGGRAPH*, pp. 11-20, 1996.
- [16] A.-Y. Shum, M. Han, and R. Szeliski, "Interactive Construction of 3D Models from Panoramic Mosaics," *Proc. IEEE CS Conf. Computer Vision and Pattern Recognition*, pp. 427-433, 1998.
- [17] E. Delage, H. Lee, and A.Y. Ng, "Automatic Single-Image 3D Reconstructions of Indoor Manhattan World Scenes," *Proc. Int'l Symp. Robotics Research*, pp. 305-321, 2005.
- [18] D. Hoiem, A. Efros, and M. Herbert, "Automatic Photo Pop-Up," *ACM Trans. Graphics*, vol. 24, no. 3, pp. 577-584, 2005.
- [19] E. Delage, H. Lee, and A. Ng, "A Dynamic Bayesian Network Model for Autonomous 3D Reconstruction from a Single Indoor Image," *Proc. IEEE CS Conf. Computer Vision and Pattern Recognition*, pp. 2418-2428, 2006.
- [20] S.K. Nayar and Y. Nakagawa, "Bubbles: A New Technique to Reveal the Use of Visual Information in Recognition Tasks," *IEEE Trans. Pattern Analysis and Machine Intelligence*, vol. 16, no. 8, pp. 824-831, 1994.
- [21] A. Criminisi, I. Reid, and A. Zisserman, "Single View Metrology," *Int'l J. Computer Vision*, vol. 40, no. 2, pp. 123-148, 2000.
- [22] A. Saxena, S.H. Chung, and A.Y. Ng, "3-D Depth Reconstruction from a Single Still Image," *Int'l J. Computer Vision*, vol. 76, no. 1, pp. 83-69, 2008.
- [23] A. Saxena, S.H. Chung, and A.Y. Ng, "Make3D: Learning 3D Scene Structure from a Single Still Image," *IEEE Trans. Pattern Analysis and Machine Intelligence*, vol. 31, no. 5, pp. 824-840, May 2009.
- [24] G. Miller, "Efficient Algorithms for Local and Global Accessibility Shading," *Proc. ACM SIGGRAPH*, pp. 319-326, 1994.
- [25] P. Cignoni, C. Montani, and R. Scopigno, "Computer-Assisted Generation of Bas- and High-Reliefs," *J. Graphics Tools*, vol. 3, no. 4, pp. 15-28, 1997.
- [26] J. Kerber, A. Belyaev, and H.-P. Seidel, "Feature Preserving Depth Compression of Range Images," *Proc. 23rd Spring Conf. Computer Graphics*, pp. 110-114, 2007.
- [27] T. Weyrich, J. Deng, C. Barnes, S. Rusinkiewicz, and A. Finkelstein, "Digital Bas-Relief from 3D Scenes," *Proc. ACM SIGGRAPH*, vol. 26, no. 3, Aug. 2007.
- [28] W. Song, A. Belyaev, and H.-P. Seidel, "Automatic Generation of Bas-Reliefs from 3D Shapes," *Proc. IEEE Int'l Conf. Shape Modeling and Applications*, pp. 211-214, 2007.
- [29] J. Kerber, A. Tevs, A. Belyaev, R. Zayer, and H.-P. Seidel, "Feature Sensitive Bas Relief Generation," *Proc. IEEE Int'l Conf. Shape Modeling and Applications*, pp. 148-154, 2009.
- [30] X. Sun, P.L. Rosin, P.R. Martin, and F.C. Langbein, "Bas-Relief Generation Using Adaptive Histogram Equalization," *IEEE Trans. Visualization and Computer Graphics*, vol. 15, no. 4, pp. 642-653, July/Aug. 2009.
- [31] M. Kass, A. Witkin, and D. Terzopoulos, "Snakes: Active Contour Models," *Int'l J. Computer Vision*, vol. 1, no. 4, pp. 321-331, 1988.
- [32] M.I.G. Bloor and M.J. Wilson, "Using Partial Differential Equations to Generate Free-Form Surfaces," *Computer-Aided Design*, vol. 22, no. 4, pp. 202-212, 1990.
- [33] M. Desbrun, M. Meyer, P. Schröder, and A.H. Barr, "Implicit Fairing of Irregular Meshes Using Diffusion and Curvature Flow," *Proc. ACM SIGGRAPH*, pp. 317-324, 1999.
- [34] R. Schneider and L. Kobbelt, "Generating Fair Meshes with G1 Boundary Conditions," *Proc. Geometric Modeling and Processing*, pp. 251-261, 2000.
- [35] G. Taubin, "A Signal Processing Approach to Fair Surface Design," *Proc. ACM SIGGRAPH*, pp. 351-358, 1995.
- [36] A. Yamada, T. Furuhashi, K. Shimada, and K.-H. Hou, "A Discrete Spring Model for Generating Fair Curves and Surfaces," *Proc. Pacific Conf. Computer Graphics and Applications*, pp. 270-279, 1999.
- [37] M. Botsch and L. Kobbelt, "An Intuitive Framework for Real-Time Freeform Modeling," *ACM Trans. Graphics*, vol. 23, no. 3, pp. 630-634, 2004.
- [38] O. Sorkine, Y. Lipman, D. Cohen-Or, and M. Alexa, "Laplacian Surface Editing," *Proc. Eurographics/ACM SIGGRAPH Symp. Geometry Processing (SGP '04)*, pp. 175-184, 2004.
- [39] M. Alexa, "Differential Coordinates for Local Mesh Morphing and Deformation," *The Visual Computer*, vol. 19, no. 2, pp. 105-114, 2003.

- [40] O. Sorkine, D. Cohen-Or, and S. Toledo, "High-Pass Quantization for Mesh Encoding," *Proc. Eurographics/ACM SIGGRAPH Symp. Geometry Processing*, pp. 42-51, 2003.
- [41] Y. Lipman, O. Sorkine, D. Cohen-Or, D. Levin, C. Rössl, and H.-P. Seidel, "Differential Coordinates for Interactive Mesh Editing," *Proc. Shape Modeling Int'l*, pp. 181-190, 2004.



Zhuwen Li received the bachelor's degree in computer science from Tianjin University, China, in 2008. Currently, he is working toward the master's degree at the State Key Lab of CAD&CG, Zhejiang University, China. His research interests include multi-view stereo, image-based modeling, shape analysis, and shape editing.



Song Wang received the BSc and MSc degrees in computer science from Huazhong Normal University, China, in 2000 and 2003, respectively. Since then, he has been a lecturer of computer science at Zhejiang University of Technology. Currently, he is working toward the PhD degree at the State Key Lab of CAD&CG, Zhejiang University, China. His research interests include computer vision, image processing, and pattern recognition.



Jinhui Yu received the BSc and MSc degrees in electronics engineering from Harbin Shipbuilding Engineering Institute, Harbin Engineering University, China, in 1982 and 1987, respectively. He received the PhD degree in computer graphics from the University of Glasgow in 1999. He is a professor of computer science at the State Key Lab of CAD&CG, Zhejiang University, China. His research interests include image-based modeling, nonphotorealistic rendering, computer animation, and computer graphics art.



Kwan-Liu Ma received the PhD degree in computer science from the University of Utah in 1993. He is a professor of computer science and the chair of the Graduate Group in Computer Science (GGCS) at the University of California, Davis. He leads the VIDI research group and directs the DOE SciDAC Institute for Ultrascale Visualization, which involves researchers from three other universities and two DOE national laboratories. His research interests include visualization, high-performance computing, and user interface design. He was a paper chair of the IEEE Visualization Conference in 2008 and 2009, and he was the founder of the IEEE Pacific Visualization Symposium. He presently serves on the editorial boards of the *IEEE Computer Graphics and Applications*, the *IEEE Transactions on Visualization and Computer Graphics*, and the *Journal of Computational Science and Discoveries*. He is a senior member of the IEEE.

▷ For more information on this or any other computing topic, please visit our Digital Library at www.computer.org/publications/dlib.